



# Frozen-hydrated chromatin from metaphase chromosomes has an interdigitated multilayer structure

Andrea Chicano<sup>1</sup>, Eva Crosas<sup>1,2,†</sup>, Joaquín Otón<sup>3</sup> , Roberto Melero<sup>3</sup> , Benjamin D Engel<sup>4</sup>  & Joan-Ramon Daban<sup>1,\*</sup> 

## Abstract

Cryo-electron tomography and small-angle X-ray scattering were used to investigate the chromatin folding in metaphase chromosomes. The tomographic 3D reconstructions show that frozen-hydrated chromatin emanated from chromosomes is planar and forms multilayered plates. The layer thickness was measured accounting for the contrast transfer function fringes at the plate edges, yielding a width of ~7.5 nm, which is compatible with the dimensions of a monolayer of nucleosomes slightly tilted with respect to the layer surface. Individual nucleosomes are visible decorating distorted plates, but typical plates are very dense and nucleosomes are not identifiable as individual units, indicating that they are tightly packed. Two layers in contact are ~13 nm thick, which is thinner than the sum of two independent layers, suggesting that nucleosomes in the layers interdigitate. X-ray scattering of whole chromosomes shows a main scattering peak at ~6 nm, which can be correlated with the distance between layers and between interdigitating nucleosomes interacting through their faces. These observations support a model where compact chromosomes are composed of many chromatin layers stacked along the chromosome axis.

**Keywords** chromatin higher-order structure; cryo-electron tomography; DNA packaging; metaphase chromosome structure; small-angle X-ray scattering

**Subject Categories** Chromatin, Epigenetics, Genomics & Functional Genomics; Structural Biology

**DOI** 10.15252/embj.201899769 | Received 4 May 2018 | Revised 29 November 2018 | Accepted 5 December 2018 | Published online 4 January 2019

**The EMBO Journal (2019) 38: e99769**

See also: **B Fierz** (April 2019)

## Introduction

During mitosis in eukaryotic cells, the enormously long genomic DNA molecules are densely packed within metaphase chromosomes (Daban, 2003). Nucleosomes are the basic building blocks of chromatin and constitute the first level of DNA compaction in the cell nucleus. The nucleosome core is a flat cylindrical particle formed by 1.7 superhelical turns of DNA (146 bp) wrapped around the core histone octamer (Luger *et al.*, 1997). In the chromatin filament, nucleosome cores are connected by variable lengths of linker DNA associated with histone H1. *In vitro* experiments showed that the compaction degree of the chromatin filament is extremely dependent on ionic conditions (Daban, 2011; Collepardo-Guevara & Schlick, 2012; Grigoryev & Woodcock, 2012; Luger *et al.*, 2012; Rippe, 2012; Boulé *et al.*, 2015). The 30-nm chromatin fiber is generally considered to be the second level of DNA compaction and, in particular, it is assumed that this fiber is the fundamental structural element for the packaging of DNA into chromosomes (Alberts *et al.*, 2014). Several structural models have been proposed for the organization of chromatin in metaphase chromosomes. From early transmission electron microscopy (TEM) images obtained with histone-depleted chromosomes, it was proposed that chromatin fibers form loops that are bound to a central protein scaffold (Paulson & Laemmli, 1977). However, subsequent chromosome stretching experiments in the presence of nucleases showed that chromosomes do not contain a continuous protein scaffold and it was suggested that chromatin fibers form an irregular network (Poirier & Marko, 2002). The analysis of chromosomes in different condensation stages indicated a hierarchical folding of fibers having diameters from 30 to 250 nm (Kireeva *et al.*, 2004), and studies of chromosome conformation capture suggested that mitotic chromosomes are formed by a compact array of chromatin loops (Gibcus *et al.*, 2018). In contrast to these models, the study of chromosome cryo-sections and small-angle X-ray scattering (SAXS) experiments showed that condensed chromosomes in 5 mM Mg<sup>2+</sup> do not have periodic structures larger

1 Departament de Bioquímica i Biologia Molecular, Facultat de Biociències, Universitat Autònoma de Barcelona, Barcelona, Spain

2 NCD Beamline, ALBA Synchrotron Light Source, Cerdanyola del Vallès, Barcelona, Spain

3 National Center of Biotechnology (CSIC), Campus Univ. Autònoma de Madrid, Madrid, Spain

4 Department of Molecular Structural Biology, Max-Planck-Institute of Biochemistry, Martinsried, Germany

\*Corresponding author. Tel: +34 935811616; E-mail: joanramon.daban@uab.cat

†Present address: Deutsches Elektronen-Synchrotron DESY, Photon Science, Hamburg, Germany

than 11 nm (Eltsov *et al*, 2008; Nishino *et al*, 2012), indicating that chromatin is not folded as a 30-nm fiber. Instead, the authors suggested that chromatin filaments in metaphase chromosomes are highly disordered and behave like a polymer melt.

Surprisingly, it was observed using conventional TEM that the incubation of metaphase chromosomes at 37°C produced the emanation of many multilayered plates (Caravaca *et al*, 2005; Gállego *et al*, 2009). This planar structure was confirmed with electron tomography (ET) of glutaraldehyde-crosslinked metaphase chromatin adsorbed to the carbon substrate of typical TEM grids (Castro-Hartmann *et al*, 2010), and with atomic force microscopy (AFM) of uncrosslinked chromatin in aqueous solution adsorbed to mica (Gállego *et al*, 2009). Although chromatin plates are very thin [each steep in a multilayered plate has an apparent thickness of 5–6 nm (Daban, 2011)], AFM-based nanotribology and force spectroscopy showed that they are flexible and have good mechanical properties in the presence of structuring concentrations of  $Mg^{2+}$  (Gállego *et al*, 2009, 2010). However, incubation with solutions containing EDTA produced plate unfolding and emanation of chromatin fibers from plate edges (Gállego *et al*, 2009). Furthermore, it was found that fragments of chromatin fibers obtained from metaphase chromosomes digested with micrococcal nuclease associate spontaneously, forming multilaminar plates that have indistinguishable structure to plates emanated from chromosomes (Milla & Daban, 2012). These observations led to the proposal of the thin-plate model, in which metaphase chromosomes are formed by many layers stacked along the chromosome axis (Gállego *et al*, 2009; Castro-Hartmann *et al*, 2010). In this work, we used cryo-electron tomography (cryo-ET) to study the 3D structure of the plates from human metaphase chromosomes. In contrast to other microscopy techniques, the plates in these experiments were not oriented by adsorption to flat substrate surfaces; the uncrosslinked and unstained sample suspended in aqueous media containing 5 mM  $Mg^{2+}$  was immobilized in vitreous ice and imaged under cryogenic conditions. In order to achieve the maximum imaging resolution and contrast (Fernandez-Leiro & Scheres, 2016), tomograms were acquired with a direct electron detector and a Volta phase plate (Danev *et al*, 2014). Furthermore, to study the internal structure of highly compacted chromosomes in the presence of the cation concentrations corresponding to metaphase [17 mM  $Mg^{2+}$  (Strick *et al*, 2001)], we took advantage of the high photon fluxes of third-generation synchrotron radiation sources (García-Gutiérrez & Rueda, 2009) to obtain SAXS data directly from whole chromosomes. Our cryo-ET and SAXS results strengthen previous evidence indicating that chromatin in metaphase chromosomes is organized as stacked mononucleosome layers that are interdigitated with each other.

## Results

### Cryo-tomograms of chromatin emanated from metaphase chromosomes

Chromosomes purified by centrifugation on sucrose step gradients in 5 mM  $Mg^{2+}$  (Fig 1A) were unfolded using the soft treatments described in the Materials and Methods. The resulting sample was deposited on EM grids coated with perforated carbon film, rapidly frozen and imaged using cryo-ET. 2D slices through the 3D

reconstructed tomographic volumes showed numerous lines of different shapes and orientations (Fig 1B). These lines in the  $x$ - $y$  plane persist along the  $z$ -axis (Fig 1C), indicating that they correspond to slices of planar structures (see the inset in Fig 1B). Although we observed planar structures adopting a variety of orientations within the ice, the tomographic missing-wedge causes anisotropic resolution (Lucic *et al*, 2005); planar structures approximately parallel to the  $x$ - $y$  plane are not well resolved, whereas those that are roughly perpendicular to the  $x$ - $y$  plane can be easily analyzed following the successive slices of the tomograms. Segmentation revealed the 3D architecture of the planar structures, which had a variety of dimensions and shapes (Fig 1C–G). We observed large plates spanning  $> 1 \mu\text{m}$  in the  $x$ - $y$  plane. The height (in the  $z$ -axis) of many plates was 0.2–0.4  $\mu\text{m}$ , which corresponds to the ice thickness in our preparations. In comparison with their large surface area, plates are very thin ( $\sim 7.5$  nm, see below), suggesting that the different sizes and shapes observed for 3D reconstructed plates are due to breakages and deformations produced during the preparation and deposition procedures. Thin plates emanated from chromosomes were observed previously using conventional TEM and AFM (Caravaca *et al*, 2005; Gállego *et al*, 2009; Castro-Hartmann *et al*, 2010). Note that in these previous experiments, samples were deposited on carbon films and mica surfaces. In contrast, in our cryo-ET experiments, the frozen-hydrated chromatin plates were not adsorbed to a flat surface, but rather suspended in vitreous ice. Therefore, the cryo-ET results show that chromatin emanated from chromosomes has an intrinsic planar geometry.

In addition to plates, we observed irregular aggregates and occasionally circular structures that have a diameter of  $\sim 30$  nm (indicated with S in Fig 2A; see also the bottom-left insets). As shown in previous studies performed with chromatin fragments (Bartolomé *et al*, 1994, 1995; Bermúdez *et al*, 1998; Daban & Bermúdez, 1998) and nucleosome arrays (Robinson *et al*, 2006), these circular structures likely correspond to cross-sections of 30-nm chromatin fibers folded as highly compact solenoids in which nucleosomes are tightly packed and cannot be distinguished as separate units. According to these studies, the dense annular zone of these structures is formed by nucleosomes of adjacent helical turns that are interdigitated (Daban & Bermúdez, 1998; Robinson *et al*, 2006). In our cryo-tomograms, these fibers are short (their length in the  $z$ -axis is 22–30 nm) and are probably formed by the helical folding of short chromatin fragments produced by mechanical breakage of the chromatin filament during the emanation of plates from soft-denatured chromosomes. We did not observe long chromatin fibers in the tomograms.

### Tight nucleosome packaging within the plates

Some chromatin plates were decorated by numerous small particles (indicated with N in Fig 2A; see also the upper-right insets in Fig 2A and the slices and segmentations of plates decorated with many small particles shown in Fig 2B–E). The size of these particles (diameter  $\sim 9$  nm; see Materials and Methods) suggests that they are nucleosomes. We performed reference-free subtomogram averaging (Briggs, 2013) with classification for a set of 902 decorative particles; different views of the most relevant class (315 particles) are shown in Fig 2F (see also Fig EV1). The lower part of the reconstructed map is the link of the particle to the plate. Although the

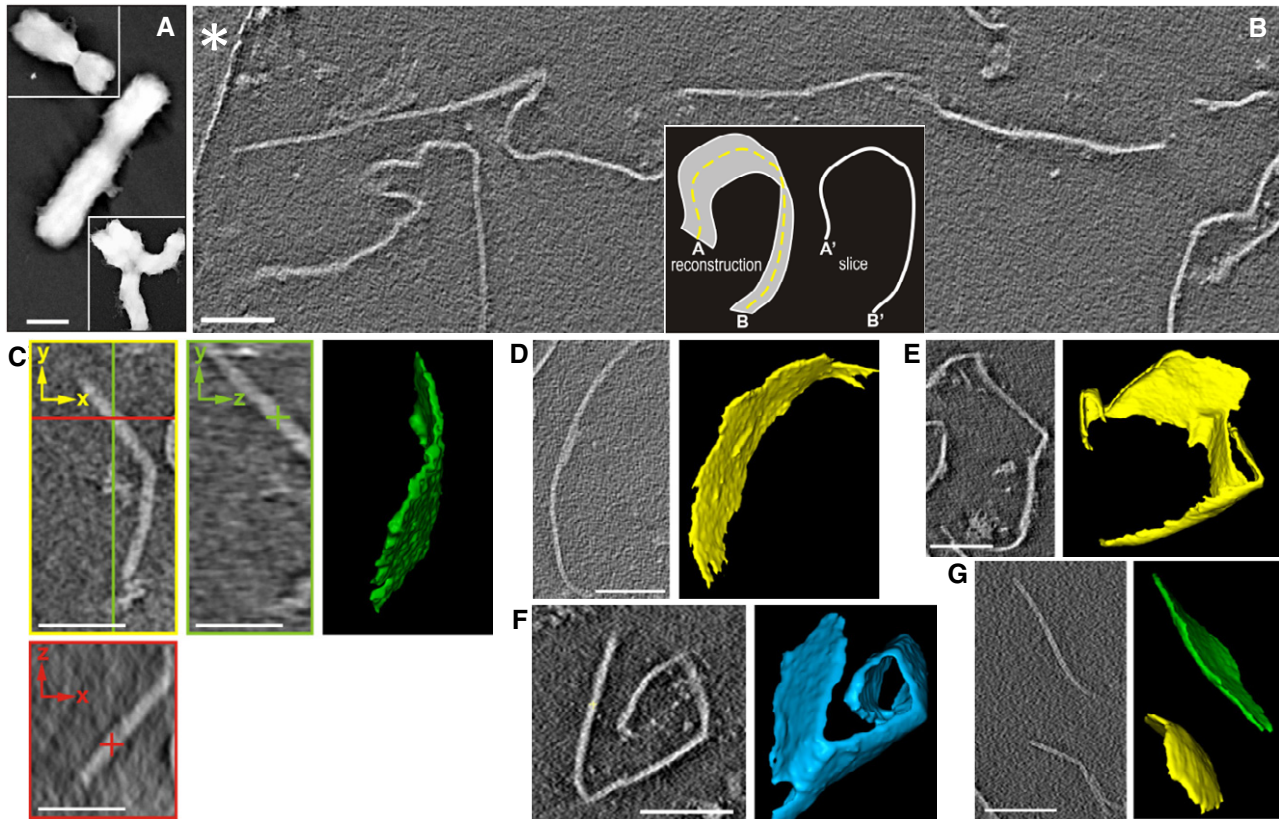


**Figure 1. Examples of cryo-tomograms containing plates emanated from metaphase chromosomes.**

A Whole chromosomes imaged by conventional TEM.

B Slice from a large tomographic volume; part of the carbon film surrounding a hole with vitrified ice containing the plates is indicated with an asterisk; the inset illustrates that the slice of a plate corresponds to a line in the  $x$ - $y$  plane (perpendicular to the direction of the electron beam).

C–G Slices from different tomograms and the corresponding 3D segmentations showing plates with different sizes and shapes. In addition to a typical slice through the  $x$ - $y$  plane (yellow), two slices through the  $x$ - $z$  (red) and  $y$ - $z$  (green) planes (orthogonal to the  $x$ - $y$  plane) are shown in (C).

Data information: Scale bars: 1  $\mu$ m (A); 200 nm (B, D), 100 nm (E–G), 50 nm (C).

resolution of the average is low, likely due to both the small number of particles and the variety of orientations relative to the plate (see Materials and Methods), we observe that the dimensions of the average are consistent with the molecular structure of the nucleosome core particle. These results suggest that the particles decorating the plates shown in Fig 2 correspond to irregularly oriented nucleosomes, which were probably extruded from distorted plates.

The distorted plates (P1 in Fig 2A; see also the upper-right insets) are relaxed and have less contrast than the typical compact plates observed in the cryo-tomograms (P2 in Fig 2A; see also Figs 1 and 4), indicating that compact plates may have a higher nucleosome concentration. The thickness of these compact plates was  $\sim 7.5$  nm (Table 1), measured directly from the tomographic slices while accounting for the contrast transfer function (CTF) fringes that border each plate (see Fig EV2). Compact plates do not show nucleosomes visible as separate units but, considering the dimensions of the nucleosome core particle (cylinder of 5.7 nm height and 11 nm diameter; Luger *et al*, 1997), the observed thickness suggests that each plate consists of a monolayer of nucleosomes aligned slightly tilted relative to the plate surface. These results indicate that compact plates are likely composed of tightly packed nucleosomes,

which may have preferred orientations within the plate. In contrast, the relaxed plates have no well-defined surfaces (compare P1 and P2 in Fig 2A), so they may contain loosely organized nucleosomes with more variable orientations.

### Plates with many stacked layers

In the cryo-tomograms, there are regions containing many parallel lines (see examples in Fig 3A and B). Each line persists in many consecutive slices along the  $z$ -axis, indicating that these structures correspond to stacked plates oriented perpendicular to the  $x$ - $y$  plane. Our measurements of several structures containing parallel lines indicated lengths in the  $z$ -axis ranging from 70 nm up to values approaching the ice thickness. The layers in the stacks have a thickness of  $\sim 7$  nm (see Materials and Methods), which is equivalent to that observed for monolayer plates (Table 1).

Figure 3C shows a slice from a tomographic volume that contains a particularly large structure formed by many stacked layers. Figure EV3 shows additional examples of large multilayer structures. According to the thin-plate model (Gállego *et al*, 2009; Castro-Hartmann *et al*, 2010), chromosomes are formed by many stacked



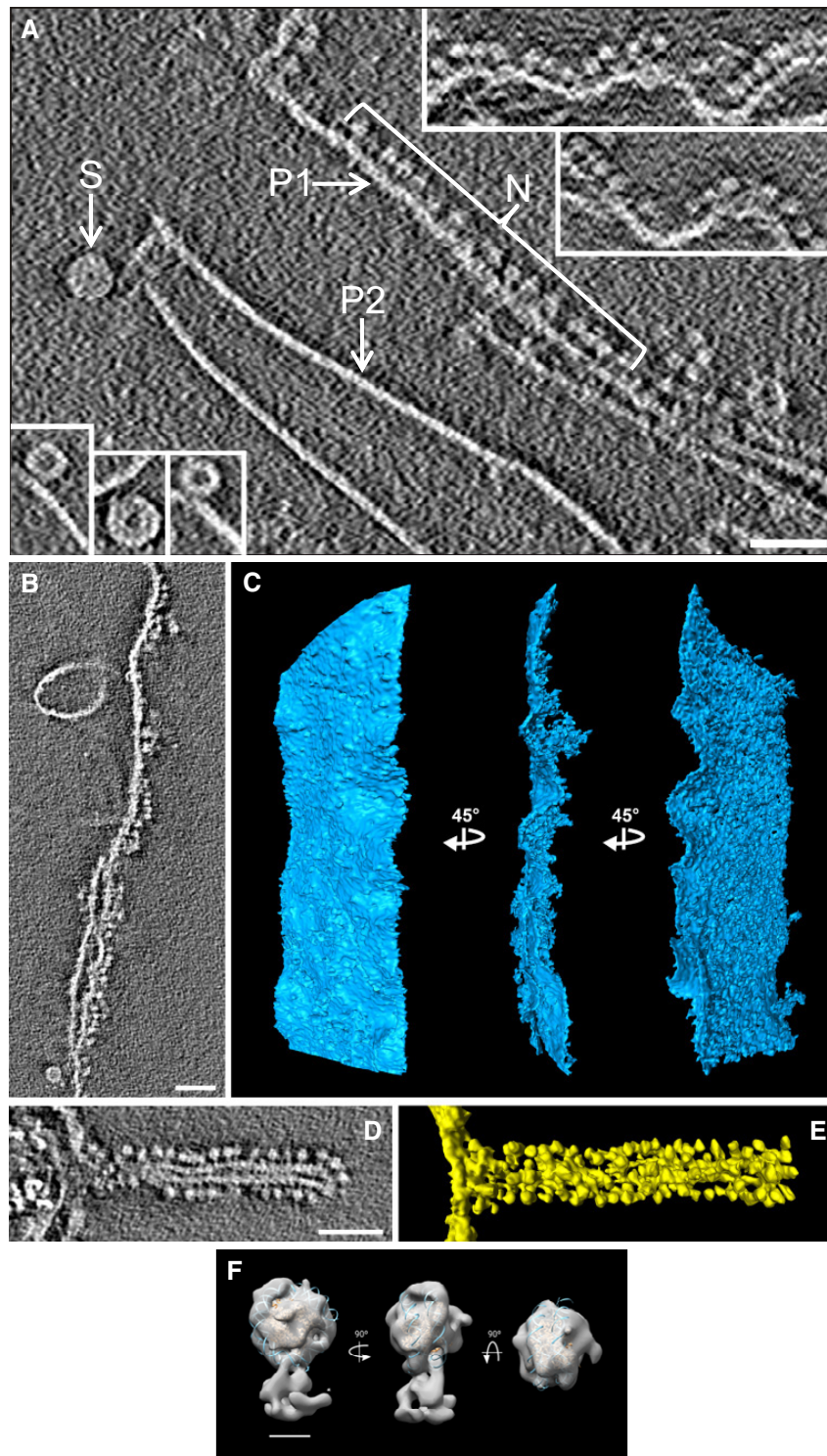


**Figure 2. Cryo-tomograms of compact plates and distorted plates decorated with nucleosomes.**

A Nucleosomes (N) decorating a relaxed plate (P1); insets in the upper right show additional examples. Nucleosomes are not visible as individual units in typical compact plates (P2). Short compact interdigitated solenoids are shown in the main image (S) and in the bottom-left insets.

B–E Slice (B) and segmentations in three different orientations (C) of a large relaxed plate decorated with many nucleosomes on its right side. Slice (D) and segmentation (E) of a relaxed plate forming a tube decorated with nucleosomes.

F Structure of the decorative particles (like those shown in N, panel A) after subtomogram averaging. The final density map was filtered to 25 Å and fitted with the molecular structure of the nucleosome core particle (Protein Data Bank code 2CV5).

Data information: Scale bars: 50 nm (A, including the insets, B–E); 5 nm (F).

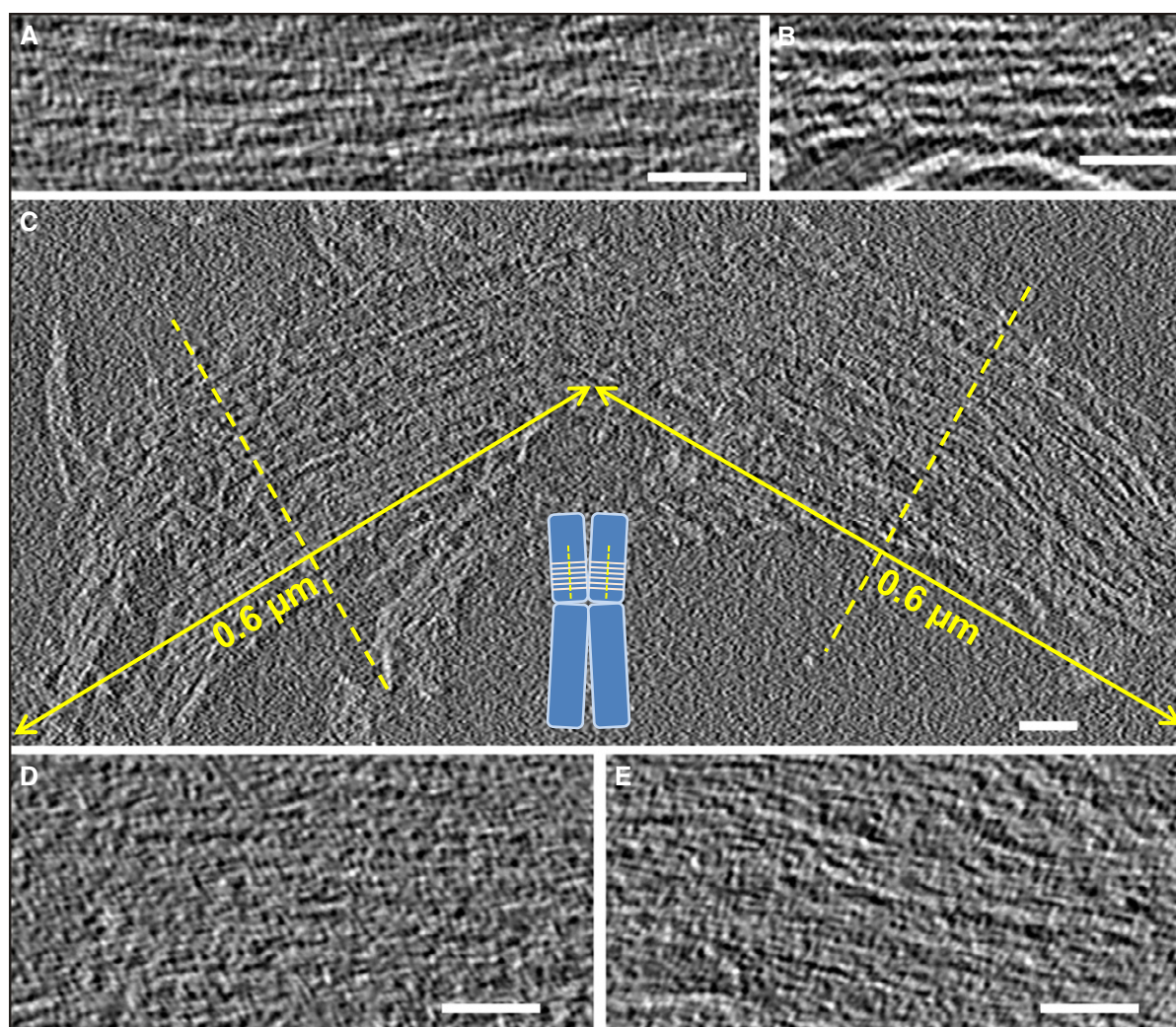
**Table 1. Plate thickness.**

Plate	Microscope <sup>a</sup>	Phase plate	Binning	Thickness <sup>b</sup> (nm)
Monolayer	Polara	–	No	7.2 ± 1.4 (n = 87)
	Polara	–	4×	8.8 ± 2.0 (n = 85)
	Krios	+	4×	7.2 ± 1.0 (n = 366)
	Krios	–	4×	7.3 ± 0.9 (n = 39)
Two layers in contact	Polara	–	No	13.0 ± 2.0 (n = 26)
	Krios	+	4×	12.4 ± 1.7 (n = 126)
	Krios	–	4×	13.0 ± 1.1 (n = 13)

<sup>a</sup>Tecnai Polara (27,500×); Titan Krios (33,000×).

<sup>b</sup>Thickness measurements account for CTF fringes as described in Fig EV2. Values shown are means ± SD of the indicated number (n) of independent measurements.

layers of chromatin oriented perpendicular to the axes of the chromatids (inset in Fig 3C); each chromatid of a human metaphase chromosome has a diameter of ~ 0.6 μm (Daban, 2014). Therefore, the dimensions of the structures in Fig EV3 suggest that they could be fragmented parts of chromatids. In the particular case of the multilayered structures in Fig 3C, since the left and right regions are apparently in contact, it is tempting to speculate that these two regions could correspond to stacked layers of two sister chromatids that broke apart during the preparation and deposition procedures. In the tomographic slice shown in this figure, parts of the layers can be seen separated from each other. However, in other slices of the same tomographic volume, the layers are much closer together and cannot be distinguished as separate units. For example, in the slices presented in Fig 3D and E (which correspond, respectively, to the left and right parts of the structure shown in Fig 3C), the layers are

**Figure 3. Slices from tomographic volumes containing multilayered plates.**

A, B Plates with several layers that are not closely appressed.

C–E Large multilayer plates having the size of human metaphase chromatids [~ 0.6 μm diameter (Daban, 2014)] (C); the inset schematically shows the perpendicular orientation of chromatin layers with respect to the chromatid axes proposed in the thin-plate model (Gállego et al, 2009; Castro-Hartmann et al, 2010). In other slices (D, E), the multilayer structures shown in (C) are more compact and the individual layers are not visible as separate elements.

Data information: Scale bars: 50 nm.



closely associated and, even at the high magnification used in these images, the structure is so compact that it is very difficult to distinguish individual layers.

### Layer interdigitation

In compact multilayered structures such as those presented in Fig 3D and E, it is not possible to analyze the structural details of the interaction between layers. Fortunately, in many tomographic volumes there are plates that interact with other plates in local regions that can be more readily analyzed. Figure 4A–C shows several examples of plates that make two-layer contacts. Taking into account that the thickness of a monolayer plate is  $\sim 7.5$  nm (Table 1), the expected thickness of two stacked layers should be  $\sim 15$  nm. However, our measurements indicate that the thickness of two layers in close contact is  $\sim 13$  nm (Table 1). These differences could be explained by a certain degree of interdigitation ( $\sim 2$  nm) between the two contacting layers. This structural solution was suggested previously from TEM and ET observations of dehydrated metaphase chromatin (Gállego *et al*, 2009; Castro-Hartmann *et al*, 2010). Density profiles across interacting layers (Fig EV4) show that the layers are in such close contact that there is no empty space between them. Interdigitation would allow face-to-face interactions between nucleosomes in adjacent layers (see below).

In addition to lateral associations, plates can also interact through their edges to form closed structures. For instance, there are circular densities in the tomographic slices shown in Fig 4A–C. The 3D segmentation presented in Fig 4D shows that the observed circles correspond to slices of plates that form cylindrical structures. Additionally, Fig 2D and E shows a plate forming a tube decorated with nucleosomes. According to previous modeling studies (Daban,

2014), the lateral interaction between plates (inter-layer association), as well as the edge-to-edge intra-layer associations, can be interpreted considering that chromatin structures with nucleosomes exposed to the aqueous medium are less stable than structures in which there are more nucleosome-nucleosome interactions. Both inter- and intra-layer associations occur because there is a stabilization of the resulting structures due to the reduction of the number nucleosomes exposed to the medium.

### SAXS analysis of condensed metaphase chromosomes

Whole metaphase chromosomes are large structures that are too dense and thick to observe chromatin organization using standard TEM (Fig 1A). To circumvent this problem, we analyzed the structure of thin chromatin plates emanated from soft-denatured metaphase chromosomes using cryo-ET (see the preceding sections), and we applied synchrotron SAXS to investigate the chromatin structure within whole intact chromosomes (Fig 5). The scattering study was performed using different divalent and trivalent cations that produce chromosome condensation (Strick *et al*, 2001; Poirier *et al*, 2002; Caravaca *et al*, 2005; Daban, 2011; Allahverdi *et al*, 2015; Maeshima *et al*, 2018). The peaks at  $\sim 3.7$  and  $\sim 2.7$  nm corresponding to the internal nucleosome structure (Widom & Klug, 1985) were observed in all samples with different intensities. The peak at  $\sim 30$  nm, which is characteristic of side-by-side packaging of 30-nm fibers (Widom, 1986), was only observed in the case of chromosomes prepared under relatively low  $Mg^{2+}$  concentration (Fig 5C). Nishino *et al* (2012) obtained a similar SAXS profile with metaphase chromosomes in 5 mM  $Mg^{2+}$ , and these authors demonstrated that the 30-nm peak can be eliminated by further chromosome purification. According to Strick *et al* (2001), in addition to physiological

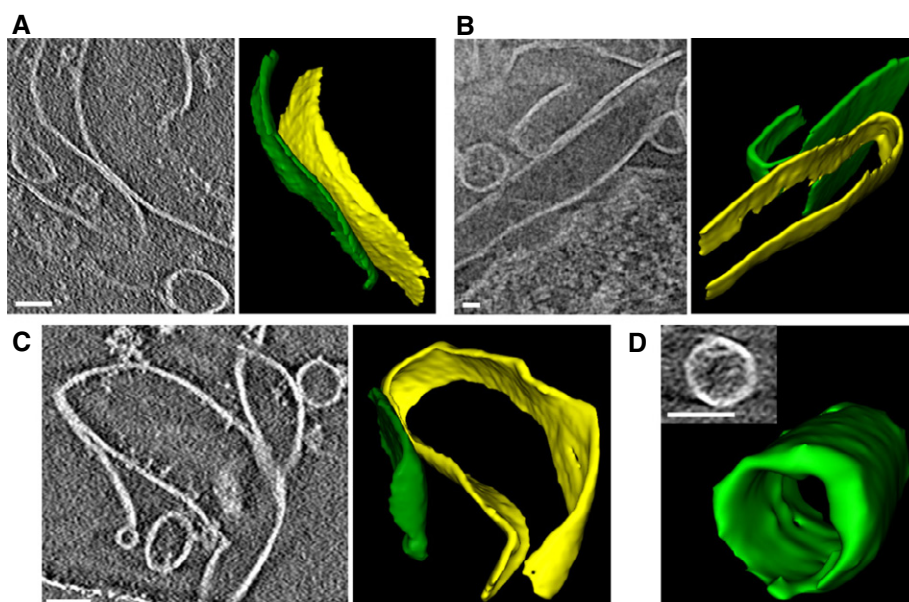


**Figure 4. Cryo-tomograms of plates showing two-layer contacts and edge-to-edge interactions.**

A–C Slices showing lateral association between two plates and the corresponding 3D segmentations.

D Edge-to-edge interactions form cylindrical structures.

Data information: Scale bars: 50 nm.

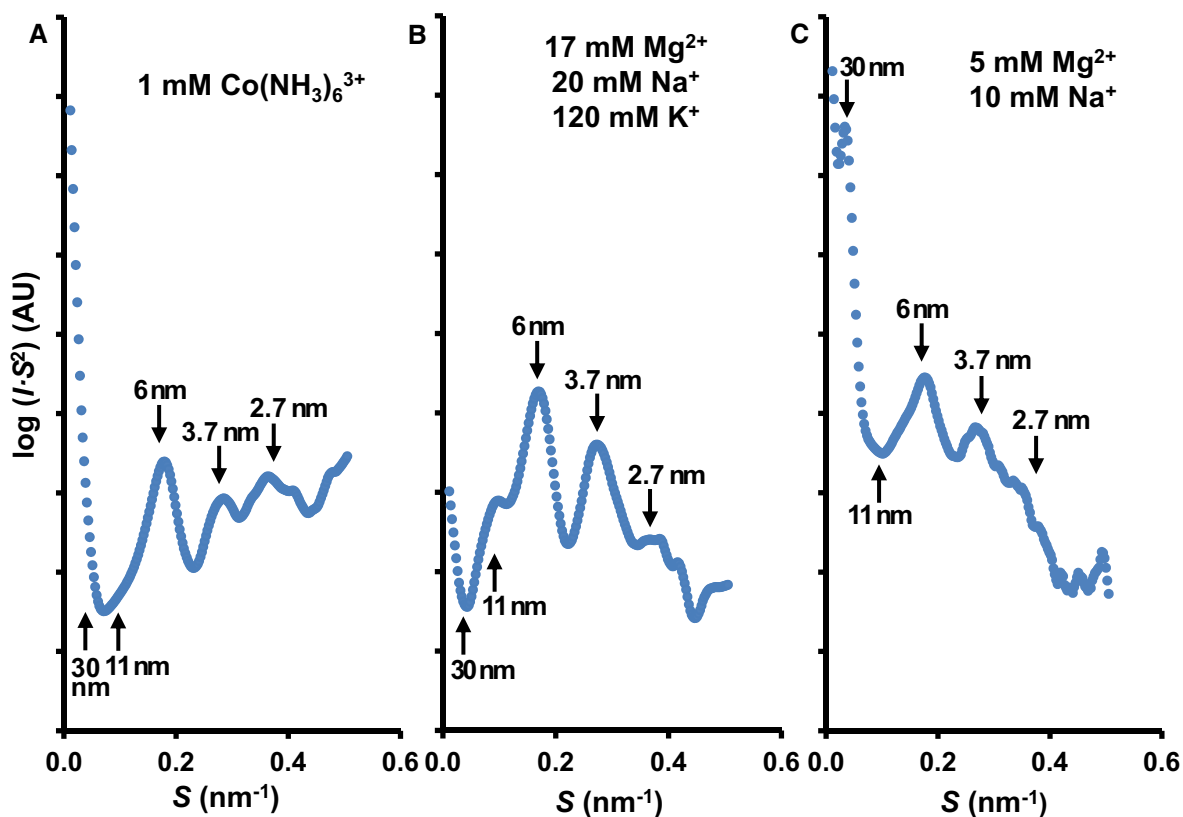


**Figure 5. SAXS profiles of metaphase chromosomes under different conditions.**

A–C The cation concentrations used are indicated for each experiment; AU, arbitrary units.

concentrations of  $K^+$  and  $Na^+$ , metaphase chromosomes contain  $\sim 17$  mM  $Mg^{2+}$  distributed homogeneously throughout the whole chromosome. Using these ionic conditions (Fig 5B), we observed that the 30-nm peak was completely absent and the peak at  $\sim 6$  nm was dominant. Similar results were obtained using the trivalent cation hexamminecobalt (Fig 5A).

As can be seen in Fig 5A–C, in all the examined structuring conditions, the scattering intensity at  $\sim 11$  nm is small compared to the prominent peak centered at  $\sim 6$  nm. According to the X-ray diffraction patterns observed for associated nucleosome cores that form columns (Mangenot *et al*, 2003; Bertin *et al*, 2007; Berezhnoy *et al*, 2016), the 6-nm peak corresponds to the distance between nucleosome cores interacting face-to-face within the columns, and the 11-nm peak is related to the distance between parallel columns (i.e., the distance corresponding to edge-to-edge nucleosome contacts). Narrow diffraction peaks were found in crystalline aggregates of nucleosome columns (Mangenot *et al*, 2003; Berezhnoy *et al*, 2016). Aggregates of nucleosome columns lacking the long-range order of crystalline structures produce broad peaks (Mangenot *et al*, 2003). Therefore, in chromosomes formed by many stacked layers, the large number of face-to-face contacts that can be produced between nucleosomes in interdigitated layers can justify the broad peak at  $\sim 6$  nm. Furthermore, this peak could also be related to the distance between stacked layers in condensed chromosomes ( $\sim 6$  nm; see Fig 6). This repeated distance strengthens the scattering peak at  $\sim 6$  nm, and this can explain why the expected

peak at  $\sim 11$  nm corresponding to edge-to-edge contacts between nucleosomes in the compact multilayered structures has a low intensity in comparison with the 6-nm peak. The scheme in Fig 6 integrates both the SAXS results and the main results obtained in the cryo-ET experiments.

## Discussion

Our tomographic 3D reconstructions show that the chromatin filament in metaphase chromosomes is organized as a planar structure that forms many layers. This chromatin folding is completely different from the 30-nm fiber proposed by many authors as the fundamental structural element of metaphase chromosomes. The chromatin emanated from soft-denatured chromosomes forms monolayer plates (Fig 1B–G), plates containing two layers in close contact (Fig 4A–C), and multilayered plates (Figs 3 and EV3). Eltsov *et al* (2008) reported that 30-nm fibers were not present in the cryo-sections of chromosomes within mitotic cells. In principle, this observation is in agreement with our results, but these authors did not observe any higher-order structure in their vitreous sections and concluded that the chromatin filament in metaphase chromosomes is completely disordered. Nevertheless, there is an alternative interpretation of these observations that is consistent with our findings: Chromatin plates cannot be distinguished as differentiated structural units in condensed chromosome cryo-sections because, as can be

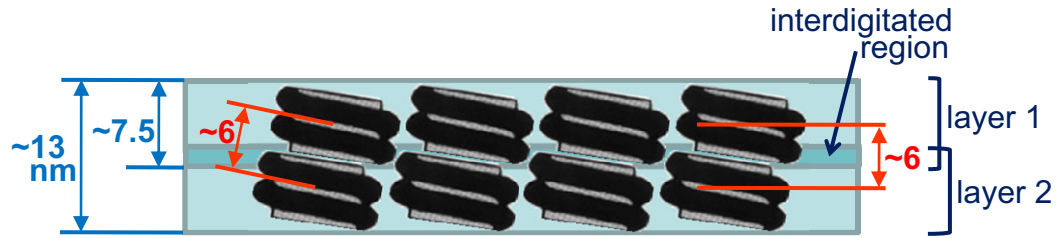


**Figure 6. Schematic drawing showing the main structural elements of two layers in close contact.**

Only a few nucleosomes are shown to illustrate the main dimensions and the interdigitation of two layers. Our results suggest that the two turns of the nucleosomal DNA are oriented slightly tilted with respect to the axis normal to the plate surface, but they may have diverse orientations (not represented in this scheme) with respect to the other two axes of the plate. The thickness of single- and double-layer plates ( $\sim 7.5$  and  $\sim 13$  nm, respectively) obtained from cryo-tomograms (Table 1) is indicated in blue. The main scattering peak at  $\sim 6$  nm observed in SAXS experiments with condensed chromosomes under metaphase ionic conditions (Fig 5B) is probably due to the repetitive distances between nucleosomes (face-to-face interactions) and between stacked layers; these distances ( $\sim 6$  nm) are indicated in red.

seen in our cryo-tomograms (Fig 3D and E), the individual layers are not visible in the interdigitated multilaminar plates. In these densely packed structures, space is completely filled by nucleosomes and consequently there is no visible higher-order organization in the cryo-sections of whole native chromosomes. Chromatin layers are only clearly visible in regions where chromosomes are distorted (Fig 3A–C).

Our SAXS results (Fig 5B) show that chromosomes prepared using the cation concentrations corresponding to metaphase conditions are not formed by densely packed 30-nm fibers; this conclusion is in agreement with a previous SAXS study by Nishino *et al* (2012) with chromosomes in 5 mM  $Mg^{2+}$ . The intense scattering at  $\sim 6$  nm observed for native chromosomes under all the conditions analyzed (Fig 5A–C and Nishino *et al*, 2012) indicates that face-to-face association between nucleosomes (Fig 6) is a fundamental structural element of metaphase chromosomes. This is not surprising because face-to-face interactions with different degrees of overlap between nucleosomes were observed previously in different chromatin samples (purified nucleosome cores, chromatin fibers, and nucleosome arrays) using physicochemical methods (Tatchell & Van Holde, 1978), TEM (Finch *et al*, 1977; Dubochet & Noll, 1978; Bartolomé *et al*, 1994; Daban & Bermúdez, 1998; Robinson *et al*, 2006), cryo-EM (Leforestier *et al*, 1999; Robinson *et al*, 2006; Scheffer *et al*, 2012; Song *et al*, 2014; Bilokapic *et al*, 2018), and X-ray scattering (Mangenot *et al*, 2003; Bertin *et al*, 2007; Berezhnoy *et al*, 2016) and crystallography (Uberbacher & Bunick, 1985; Luger *et al*, 1997; Harp *et al*, 2000; White *et al*, 2001; Schalch *et al*, 2005; Ekundayo *et al*, 2017; Zhou *et al*, 2018); this interaction was also described in modeling studies (Stehr *et al*, 2010; Fan *et al*, 2013; Korolev *et al*, 2016, 2018; Saurabh *et al*, 2016; Ishida & Kono, 2017). The lateral association between two nucleosome cores involves an acidic surface formed by histones H2A and H2B and basic residues of the N-terminal tail of histone H4 (Luger *et al*, 1997; Harp *et al*, 2000; White *et al*, 2001; Schalch *et al*, 2005). The diversity of nucleosome orientations observed in these lateral interactions (Mangenot *et al*, 2003; Ekundayo *et al*, 2017; Ishida & Kono, 2017; Bilokapic *et al*, 2018; Korolev *et al*, 2018; Zhou *et al*, 2018) may facilitate the association of nucleosomes in adjacent layers of chromatin plates.

The dense packaging observed in multilayered structures (Fig 3D and E), and the measurements (Table 1) showing that the

thickness of two layers in close contact is smaller than the sum of two independent layers suggest that there is interdigitation between the stacked layers. This interdigitation allows face-to-face interactions of nucleosomes in adjacent layers (Fig 6). *In vitro* experiments and modeling studies demonstrated previously that interdigitation facilitates face-to-face nucleosome interactions that stabilize folded fibers with different conformations (Bartolomé *et al*, 1994; Daban & Bermúdez, 1998; Robinson *et al*, 2006; Wong *et al*, 2007; Depken & Schiessel, 2009; Rippe, 2012; Wu *et al*, 2016). The degree of interdigitation of the successive turns of compact solenoids is dependent on the orientation of the nucleosomes (Daban & Bermúdez, 1998). In agreement with this observation, our interpretation that nucleosomes are only slightly tilted within the plates explains why the observed degree of interdigitation in the multilayer plates is relatively low. Grigoryev (2004) and other authors (Eltsov *et al*, 2008; Castro-Hartmann *et al*, 2010; Daban, 2011; Grigoryev & Woodcock, 2012; Luger *et al*, 2012; Collepardo-Guevara & Schlick, 2014; Grigoryev *et al*, 2016; Maeshima *et al*, 2016; Bascom & Schlick, 2017) suggested that the lateral interdigitation of fibers can produce inter-fiber associations. *In vitro* experiments performed with diluted chromatin fragments or nucleosome arrays in the presence of low cation concentrations showed that only intra-fiber interactions between close neighbor nucleosomes can form (Eltsov *et al*, 2008; Daban, 2011); under these conditions, fibers folded as compact interdigitated solenoids (Daban & Bermúdez, 1998; Robinson *et al*, 2006) are the most complex structures that can be produced. In contrast, the high concentrations of chromatin (Daban, 2000) and cations (Strick *et al*, 2001) within condensed metaphase chromosomes allow the interaction between nucleosomes that are very distant in the single DNA molecule that is packed within each chromatid. All these observations strengthen the hypothesis that interdigitation combined with face-to-face interactions between nucleosomes in the successive layers stabilizes the multilaminar organization of planar chromatin in metaphase chromosomes.

We have performed an *in vitro* study using conditions that approach as much as possible the structuring ionic concentrations of metaphase cells, but future *in vivo* research will be required to validate the observed multilayered organization of chromatin. However, the functional role of this chromatin organization can be inferred from its structural and physical properties. The mechanical



strength of planar chromatin (Gállego *et al*, 2010) and the stability of the stacked chromatin layers in metaphase chromosomes (see above) suggest that its primary biological role is the maintenance of the integrity of genomic DNA during mitosis. Furthermore, it was shown that this chromatin organization avoids topological entanglements of the chromatin filament (Milla & Daban, 2012) and can justify the elongated cylindrical structure of chromosomes as well as their outstanding mechanical properties (Poirier *et al*, 2000; Daban, 2014). It was also shown that if chromosomes consist of many stacked layers of planar chromatin, it is possible to explain many cytogenetic observations that were not previously understood (Daban, 2015). Presumably, the typical chromosome bands are produced by the preferential staining of several chromatin layers with different dyes, and the observed transverse orientation of the bands is due to the perpendicular orientation of the chromatin layers with respect to the chromosome axis. This also explains the splitting of broad bands (formed by several layers) observed in chromosome stretching experiments (Hliscs *et al*, 1997), and the maintenance of the orthogonal orientation of the split bands. According to the local concentration of DNA in metaphase chromosomes ( $\sim 170 \text{ Mb}/\mu\text{m}^3$ ; Daban, 2000, 2014), each chromatin layer of a human chromosome is formed by  $\sim 0.5 \text{ Mb}$  of DNA, which justifies the existence of very thin bands containing  $< 1 \text{ Mb}$  (International Human Genome Sequencing Consortium, 2001). The multilayered structure of chromatin in metaphase chromosomes is also compatible with the orthogonal orientation and planar structure of the connection surfaces seen in sister chromatid exchanges, and in the translocations observed in cancer cells. It has been argued (Daban, 2015) that the fibrillar models proposed by other authors (Paulson & Laemmli, 1977; Poirier & Marko, 2002; Kireeva *et al*, 2004; Eltsov *et al*, 2008; Naumova *et al*, 2013) require large quantities of DNA to cover the chromosome cross-section and cannot justify the existence of very thin orthogonal bands and the orthogonal orientation of the connection surfaces in chromosome rearrangements.

There are several chromosome conformation capture methods capable of identifying contacts between distant regions of the chromatin filament via chemical crosslinking (Sajan & Hawkins, 2012; Bonev & Cavalli, 2016). In the genome-wide Hi-C method, the cross-linked contacting regions are identified by high-throughput sequencing (Lieberman-Aiden *et al*, 2009). Recently, Hi-C results obtained with mitotic cells were modeled using polymer-based simulations of chromatin structure, and it was proposed that chromatin in mitotic chromosomes is folded as a compact array of many loops having different sizes during mitosis (Gibcus *et al*, 2018). In the model proposed by these authors, the final compact chromosomes are formed by loops of  $\sim 0.5 \text{ Mb}$  (consisting of  $\sim 400\text{-kb}$  outer loops and  $\sim 80\text{-kb}$  inner loops) and have a linear density of  $\sim 60 \text{ Mb}/\mu\text{m}$ . For chromatids with a radius of  $\sim 0.36 \mu\text{m}$  (Gibcus *et al*, 2018), this linear density corresponds to  $\sim 150 \text{ Mb}/\mu\text{m}^3$ . This local DNA concentration is similar to the value considered above for multilayered chromosomes ( $\sim 170 \text{ Mb}/\mu\text{m}^3$ ; Daban, 2000, 2014) and is compatible with the high chromatin density observed for metaphase chromosomes by other authors (Eltsov *et al*, 2008; Ou *et al*, 2017). Obviously, to achieve this high density, the long chromatin filament in each  $0.5\text{-Mb}$  loop cannot be extended and must be tightly packed. We propose that the chromatin in the loops detected in the Hi-C studies could be compacted into the multilayered plates observed in this work.

## Materials and Methods

### Preparation of metaphase chromosomes and chromatin plates

Chromosomes from HeLa cells blocked in metaphase with colcemid were prepared in TE buffer (15 mM triethanolamine-HCl, pH 7.4, 2 mM EDTA, 0.5 mM EGTA, 20 mM NaCl, 80 mM KCl, 0.2 mM spermine, 0.5 mM spermidine, and 0.5% Triton X-100) as described previously (Caravaca *et al*, 2005; Gállego *et al*, 2009); for SAXS experiments in the presence of 5 mM  $\text{Mg}^{2+}$ , chromosomes were prepared in 10 mM PIPES (pH 7.2), 10 mM NaCl, 5 mM  $\text{Mg}^{2+}$ , and 0.5% Triton X-100. Chromosome suspensions were centrifuged at 4,000 *g* for 5 min. The resulting pellets were washed twice at 4°C with 10 mM PIPES (pH 7.2), 40% glycerol, and the concentrations of cations indicated in Fig 5. Finally, the samples were transferred to plastic capillaries (2 mm diameter, MiTeGen) and stored at  $-80^\circ\text{C}$  for further SAXS measurements. For the preparation of chromatin plates, chromosomes in TE buffer (containing 1 mg/ml digitonin instead of Triton X-100) were purified on a sucrose step gradient, with four layers (30, 40, 50, and 60% sucrose) containing 5 mM PIPES (pH 7.2), 5 mM NaCl, and 5 mM  $\text{MgCl}_2$  (PM buffer). Chromosomes were collected from the 40–50% and 50–60% sucrose interfaces; TEM images of these chromosomes were obtained following previously described procedures (Castro-Hartmann *et al*, 2010). The chromosome suspension was diluted with four volumes of PM buffer without sucrose, passed several times through a 22-gauge syringe needle, and finally dialyzed for 2.5 h at 37°C against the same buffer without sucrose. Each one of these treatments applied separately favors the emanation of chromatin plates from chromosomes (Gállego *et al*, 2009; Castro-Hartmann *et al*, 2010), but we applied the three methods to obtain a high yield of plates. Note that in order to preserve the native chromatin structure as much as possible, the concentration of  $\text{Mg}^{2+}$  was maintained throughout these treatments. This sample was stored for 24 h in an ice bath and then used for the cryo-preparations.

### Cryo-ET and image analysis

Perforated carbon films (Quantifoil R2/1) on 200-mesh molybdenum grids were made hydrophilic by glow discharge before sample deposition. 200  $\mu\text{l}$  of sample was pipetted onto the grid (placed in the cap of an inverted tube) and centrifuged at 1,500 *g* for 10 min. The grid was placed in a VitroBot Mark III (set to 22°C and 95% humidity; blot offset  $-3 \text{ mm}$ ), 2  $\mu\text{l}$  of gold particles (Aurion BSA tracers) in PM buffer were added, and the grid was blotted for 6 s from the reverse side and immediately plunged into a liquid ethane/propane mixture at liquid nitrogen temperature. Frozen-hydrated preparations were stored in liquid nitrogen until used. Two sets of tomograms were obtained at the Instruct cryo-ET platform at Max-Planck-Institute of Biochemistry (Martinsried). The first set (seven tomograms) was obtained with a Tecnai G2 Polara (FEI) microscope and the second set (25 tomograms) with a Titan Krios (FEI) microscope. Both instruments were equipped with field-emission guns operated at 300 kV, post-column energy filters (GIF 2002, Gatan), and K2 Summit (Gatan) direct electron-detection cameras; in addition, in the case of Titan Krios most of the tomograms were obtained using a FEI Volta phase plate (Danev *et al*, 2014). Tilt series (range  $\pm 60^\circ$ ; increments of  $2^\circ$ ) were collected

under low-dose conditions (total dose  $\sim 110 \text{ e}^-/\text{\AA}^2$ ) using SerialEM software (Mastrorarde, 2005) with  $-5$  to  $-6 \mu\text{m}$  defocus at  $27,500\times$  magnification (image pixel size of  $4.27 \text{ \AA}$ ) in the Polara, and with  $-0.5 \mu\text{m}$  defocus at  $33,000\times$  magnification (image pixel size of  $4.21 \text{ \AA}$ ) in Titan Krios equipped with the phase plate. Image frames from the K2 direct detector were aligned using in-house developed software based on the algorithm described in Li *et al* (2013). Alignment of the images of each tilt series was performed with IMOD software (Kremer *et al*, 1996) using fiducial gold particles, and tomographic 3D reconstruction was performed using the weighted back projection. Generally, to enhance contrast, tomograms were  $4\times$  binned, but in some cases (see Table 1) unbinned images were used for 3D reconstructions. Segmentations and the measurements of plate thickness and nucleosome dimensions were performed with Fiji-ImageJ (NIH). These measurements accounted for the CTF fringes bordering the plates (caused by defocus and other modulating effects), as described in Fig EV2. The thickness of monolayers and two layers in close contact is presented in Table 1. The thickness of single layers in multilayered structures is  $6.6 \pm 1.5$  ( $n = 205$ ), and the diameter of nucleosomes decorating distorted plates is  $8.7 \pm 1.3 \text{ nm}$  ( $n = 206$ ). Unless otherwise indicated, measurements were made using slices from  $4\times$  binned tomograms obtained with the Titan Krios microscope, equipped with the phase plate. The slices from tomographic volumes are shown in reverse contrast.

### Subtomogram averaging and classification

For a detailed analysis of the decorative particles (N in Fig 2A), a set of 902 particles was manually picked and extracted using the EMAN package (Tang *et al*, 2007). The subtomogram average was generated from data acquired on the Titan Krios microscope using the Volta phase plate and  $0.5\text{-}\mu\text{m}$  defocus. The 3D alignment and classification were performed using algorithms based on maximum likelihood (Scheres *et al*, 2009) included in the Xmipp package (de la Rosa-Trevín *et al*, 2013). We did not apply a focused mask, only a standard spherical mask about the same size as the box to prevent hard box edges from influencing the alignment. We processed four classes (155, 192, 315, and 240 particles) using a 50 pixel box size and 15 iterations. Classes 1, 2, and 4 resulted in noisy versions of class 3, which was filtered to  $25 \text{ \AA}$  (Fig 2F). The method is reference-free; the process was started from a weighted average structure obtained from random orientations of all particles. Figure EV1 shows the evolution of the averaged subvolume at each iteration without filtering. Two parts can be distinguished in the reconstructed volume: the top region that has the size of a nucleosome core particle and the lower region corresponding to the link of the particle to the plate. Due to the large box size, part of the plate associated with decorative nucleosomes is also included in the subtomogram average. The limited number of particles available in cryo-ET experiments did not allow to obtain a high-resolution structure; the resolution estimated using the local resolution algorithm MonoRes (Vilas *et al*, 2018) is around  $3 \text{ nm}$ .

### SAXS experiments

X-ray scattering of condensed chromosomes was recorded at room temperature at the non-crystalline diffraction (NCD) beamline of the ALBA Synchrotron (Cerdanyola del Vallès, Barcelona) using a SAXS

Quantum 210r CCD detector from ADSC. Different zones of the chromosome pellets were exposed to X-rays for 60 s. The wavelength  $\lambda$  was  $1.29 \text{ \AA}$  and the sample-to-detector distance was  $2.61 \text{ m}$ . SAXS data are shown as plots of  $\log(I/S^2)$  versus  $S$ , where  $I$  is the average intensity obtained after subtracting the buffer scattering and  $S = 2\sin\theta/\lambda$  is the scattering vector;  $2\theta$  is the scattering angle.

## Data availability

The subtomogram average of nucleosome particles decorating unstructured plates and a cryo-electron tomogram of chromatin plates emanated from metaphase chromosomes have been deposited in the Electron Microscopy Data Bank (EMDB; <http://www.emdatabank.org>) with accession numbers EMD-0117 and EMD-0119, respectively.

**Expanded View** for this article is available online.

### Acknowledgements

The authors thank the staffs of the Serveis de Microscòpia and Cultius Cellulars (UAB), the cryo-ET and image processing Instruct platforms, and the NCD-BL11 staff from ALBA Synchrotron for their invaluable assistance. This work was supported in part by MINECO research grant BFU2010-18939, European Union (EU) and Horizon 2020 through grant West-Life (EINFRA-2015-1, Proposal: 675858), and a by a UAB-PIF predoctoral fellowship to AC. Cryo-ET experiments at Max-Planck-Institute of Biochemistry (Martinsried) and image processing at National Center of Biotechnology (Madrid) were funded by Instruct (PID250, PID2115), part of the European Strategy Forum on Research Infrastructures (ESFRI) and supported by national member subscriptions.

### Author contributions

AC designed experiments, prepared chromatin plates, collected cryo-ET and SAXS data, performed image processing, and analyzed data; EC designed experiments, prepared metaphase chromosomes, and collected and analyzed SAXS data; JO and RM processed cryo-ET data and performed subtomogram averaging; BDE collected and analyzed cryo-ET data, supervised the cryo-ET experiments, and wrote the paper; J-RD conceived and supervised the project, designed experiments, analyzed cryo-ET and SAXS data, and wrote the paper.

### Conflict of interest

The authors declare that they have no conflict of interest.

## References

- Alberts B, Johnson A, Lewis J, Morgan D, Raff M, Roberts K, Walter P (2014) *Molecular biology of the cell*, pp 207–216. New York, NY: Garland Science
- Allahverdi A, Chen Q, Korolev N, Nordenskiöld L (2015) Chromatin compaction under mixed salt conditions: opposite effects of sodium and potassium ions on nucleosome array folding. *Sci Rep* 5: 8512
- Bartolomé S, Bermúdez A, Daban JR (1994) Internal structure of the 30 nm chromatin fiber. *J Cell Sci* 107: 2983–2992
- Bartolomé S, Bermúdez A, Daban JR (1995) Electrophoresis of chromatin on non-denaturing agarose gels containing  $\text{Mg}^{2+}$ . Self-assembly of small chromatin fragments and folding of the 30-nm fiber. *J Biol Chem* 270: 22514–22521

- Bascom G, Schlick T (2017) Linking chromatin fibers to gene folding by hierarchical looping. *Biophys J* 112: 434–445
- Bereznoy NV, Liu Y, Allahverdi A, Yang R, Su CJ, Liu CF, Korolev N, Nordenskiöld L (2016) The influence of ionic environment and histone tails on columnar order of nucleosome core particles. *Biophys J* 110: 1720–1731
- Bermúdez A, Bartolomé S, Daban JR (1998) Partial denaturation of small chromatin fragments: direct evidence for the radial distribution of nucleosomes in folded chromatin fibers. *J Cell Sci* 111: 1707–1715
- Bertin A, Mangelot S, Renouard M, Durand D, Livolant F (2007) Structure and phase diagram of nucleosome core particles aggregated by multivalent cations. *Biophys J* 93: 3652–3663
- Bilokapic S, Strauss M, Halic M (2018) Cryo-EM of nucleosome core particle interactions in trans. *Sci Rep* 8: 7046
- Bonev B, Cavalli G (2016) Organization and function of the 3D genome. *Nat Rev Genet* 17: 661–678
- Boulé JB, Mozziconacci J, Lavelle C (2015) The polymorphisms of the chromatin fiber. *J Phys Condens Matter* 27: 033101
- Briggs JAG (2013) Structural biology *in situ*: the potential of subtomogram averaging. *Curr Opin Struct Biol* 23: 261–267
- Caravaca JM, Caño S, Gállego I, Daban JR (2005) Structural elements of bulk chromatin within metaphase chromosomes. *Chromosome Res* 13: 725–743
- Castro-Hartmann P, Milla M, Daban JR (2010) Irregular orientation of nucleosomes in the well-defined chromatin plates of metaphase chromosomes. *Biochemistry* 49: 4043–4050
- Collepardo-Guevara R, Schlick T (2012) Crucial role of dynamic linker histone binding and divalent ions for DNA accessibility and gene regulation revealed by mesoscale modeling of oligonucleosomes. *Nucleic Acids Res* 18: 8803–8817
- Collepardo-Guevara R, Schlick T (2014) Chromatin fiber polymorphism triggered by variations of DNA linker length. *Proc Natl Acad Sci USA* 111: 8061–8066
- Daban JR, Bermúdez A (1998) Interdigitated solenoid model for compact chromatin fibers. *Biochemistry* 37: 4299–4304
- Daban JR (2000) Physical constraints in the condensation of eukaryotic chromosomes. Local concentration of DNA versus linear packing ratio in higher order chromatin structures. *Biochemistry* 39: 3861–3866
- Daban JR (2003) High concentration of DNA in condensed chromatin. *Biochem Cell Biol* 81: 91–99
- Daban JR (2011) Electron microscopy and atomic force microscopy studies of chromatin and metaphase chromosome structure. *Micron* 42: 733–750
- Daban JR (2014) The energy components of stacked chromatin layers explain the morphology, dimensions and mechanical properties of metaphase chromosomes. *J R Soc Interface* 11: 20131043
- Daban JR (2015) Stacked thin layers of metaphase chromatin explain the geometry of chromosome rearrangements and banding. *Sci Rep* 5: 14891
- Danev R, Buijsse B, Khoshouei M, Plitzko JM, Baumeister W (2014) Volta potential phase plate for in-focus phase contrast transmission electron microscopy. *Proc Natl Acad Sci USA* 111: 15635–15640
- Depken M, Schiessel H (2009) Nucleosome shape dictates chromatin fiber structure. *Biophys J* 96: 777–784
- Dubochet J, Noll M (1978) Nucleosome arcs and helices. *Science* 202: 280–286
- Ekundayo B, Richmond TJ, Schalch T (2017) Capturing structural heterogeneity in chromatin fibers. *J Mol Biol* 429: 3031–3042
- Eltsov M, MacLellan KM, Maeshima K, Frangakis AS, Dubochet J (2008) Analysis of cryo-electron microscopy images does not support the existence of 30-nm chromatin fibers in mitotic chromosomes *in situ*. *Proc Natl Acad Sci USA* 105: 19732–19737
- Fan Y, Korolev N, Lyubartsev AP, Nordenskiöld L (2013) An advanced coarse-grained nucleosome core particle model for computer simulations of nucleosome-nucleosome interactions under varying ionic conditions. *PLoS One* 8: e54228
- Fernandez-Leiro R, Scheres SHW (2016) Unravelling biological macromolecules with cryo-electron microscopy. *Nature* 537: 339–346
- Finch JT, Lutter LC, Rhodes D, Brown RS, Rushton B, Levitt M, Klug A (1977) Structure of nucleosome core particles of chromatin. *Nature* 269: 29–36
- Gállego I, Castro-Hartmann P, Caravaca JM, Caño S, Daban JR (2009) Dense chromatin plates in metaphase chromosomes. *Eur Biophys J* 38: 503–522
- Gállego I, Oncins G, Sisquella X, Fernández-Busquets X, Daban JR (2010) Nanotribology results show that DNA forms a mechanically resistant 2D network in metaphase chromatin plates. *Biophys J* 99: 3951–3958
- García-Gutiérrez MC, Rueda DR (2009) Bases of synchrotron radiation, light sources, and features of X-ray scattering beamlines. *Lect Notes Phys* 776: 1–22
- Gibcus JH, Samejima K, Goloborodko A, Samejima I, Naumova N, Nuebler J, Kanemaki MT, Xie L, Paulson JR, Earnshaw WC, Mirny LA, Dekker J (2018) A pathway for mitotic chromosome formation. *Science* 359: eaao6135
- Grigoryev SA (2004) Keeping fingers crossed: heterochromatin spreading through interdigitation of nucleosome arrays. *FEBS Lett* 564: 4–8
- Grigoryev SA, Woodcock CL (2012) Chromatin organization. The 30 nm fiber. *Exp Cell Res* 318: 1448–1455
- Grigoryev SA, Bascom G, Buckwalter JM, Schubert MB, Woodcock CL, Schlick T (2016) Hierarchical looping of zigzag nucleosome chains in metaphase chromosomes. *Proc Natl Acad Sci USA* 113: 1238–1243
- Harp JM, Hanson BL, Timm DE, Bunick GJ (2000) Asymmetries in the nucleosome core particle at 2.5 Å resolution. *Acta Crystallogr D Biol Crystallogr* 56: 1513–1534
- Hliscs R, Mühlhig P, Claussen U (1997) The nature of G-bands analyzed by chromosome stretching. *Cytogenet Cell Genet* 79: 162–166
- International Human Genome Sequencing Consortium (2001) Initial sequencing and analysis of the human genome. *Nature* 409: 860–921
- Ishida H, Kono H (2017) H4 tails potentially produce the diversity in the orientation of two nucleosomes. *Biophys J* 113: 978–990
- Kireeva N, Lakonishok M, Kireev I, Hirano T, Belmont AS (2004) Visualization of early chromosome condensation: a hierarchical folding, axial glue model of chromosome structure. *J Cell Biol* 166: 775–785
- Korolev N, Nordenskiöld L, Lyubartsev AP (2016) Multiscale coarse-grained modelling of chromatin components: DNA and the nucleosome. *Adv Colloid Interface Sci* 232: 36–48
- Korolev N, Lyubartsev AP, Nordenskiöld L (2018) A systematic analysis of nucleosome core particle and nucleosome-nucleosome stacking structure. *Sci Rep* 8: 1543
- Kremer JR, Mastrorade DN, McIntosh JR (1996) Computer visualization of three-dimensional image data using IMOD. *J Struct Biol* 116: 71–76
- Leforestier A, Fudaley S, Livolant F (1999) Spermidine-induced aggregation of nucleosome core particles: evidence for multiple liquid crystalline phases. *J Mol Biol* 290: 481–494
- Li X, Mooney P, Zheng S, Booth CR, Braunfeld MB, Gubbens S, Agard DA, Cheng Y (2013) Electron counting and beam-induced motion correction enable near-atomic-resolution single-particle cryo-EM. *Nat Methods* 10: 584–590
- Lieberman-Aiden E, van Berkum NL, Williams L, Imakaev M, Ragoczy T, Telling A, Amit I, Lajoie BR, Sabo PJ, Dorschner MO, Sandstrom R, Bernstein B, Bender MA, Groudine M, Gnirke A, Stamatoyannopoulos J,



- Mirny LA, Lander ES, Dekker J (2009) Comprehensive mapping of long-range interactions reveals folding principles of the human genome. *Science* 326: 289–293
- Lucic V, Förster F, Baumeister W (2005) Structural studies by electron tomography: from cells to molecules. *Annu Rev Biochem* 74: 833–865
- Luger K, Mäder AW, Richmond RK, Sargent DF, Richmond TJ (1997) Crystal structure of the nucleosome core particle at 2.8 Å resolution. *Nature* 389: 251–260
- Luger K, Dechassa ML, Tremethick DJ (2012) New insight into nucleosome and chromatin structure: an ordered state or a disordered affair? *Nat Rev Mol Cell Biol* 13: 436–447
- Maeshima K, Rogge R, Tamura S, Joti Y, Hikima T, Szerlong H, Krause C, Herman J, Seidel E, DeLuca J, Ishikawa T, Hansen JC (2016) Nucleosomal arrays self-assemble into supramolecular globular structures lacking 30-nm fibers. *EMBO J* 35: 1115–1132
- Maeshima K, Matsuda T, Shindo Y, Imamura H, Tamura S, Imai R, Kawakami S, Nagashima R, Soga T, Noji H, Oka K, Nagai T (2018) A transient rise in free Mg<sup>2+</sup> ions released from ATP-Mg hydrolysis contributes to mitotic chromosome condensation. *Curr Biol* 28: 1–8
- Mangenot S, Leforestier A, Durand D, Livolant F (2003) X-ray diffraction characterization of the dense phases formed by nucleosome core particles. *Biophys J* 84: 2570–2584
- Mastrorade DN (2005) Automated electron microscope tomography using robust prediction of specimen movements. *J Struct Biol* 152: 36–51
- Milla M, Daban JR (2012) Self-assembly of thin plates from micrococcal nuclease-digested chromatin of metaphase chromosomes. *Biophys J* 103: 567–575
- Naumova N, Imakaev M, Fudenberg G, Zhan Y, Lajoie BR, Mirny LA, Dekker J (2013) Organization of the mitotic chromosome. *Science* 342: 948–953
- Nishino Y, Eltsov M, Joti Y, Ito K, Takata H, Takahashi Y, Hihara S, Frangakis AS, Imamoto N, Ishikawa T, Maeshima K (2012) Human mitotic chromosomes consist predominantly of irregularly folded nucleosome fibres without a 30-nm chromatin structure. *EMBO J* 31: 1644–1653
- Ou HD, Phan S, Deerinck TJ, Thor A, Ellisman MH, O'Shea CC (2017) ChromEMT: visualizing 3D chromatin structure and compaction in interphase and mitotic cells. *Science* 357: eaag0025
- Paulson JR, Laemmli UK (1977) The structure of histone-depleted metaphase chromosomes. *Cell* 12: 817–828
- Poirier M, Eroglu S, Chatenay D, Marko JF (2000) Reversible and irreversible unfolding of mitotic newt chromosomes by applied force. *Mol Biol Cell* 11: 269–276
- Poirier MG, Marko JF (2002) Mitotic chromosomes are chromatin networks without a mechanically contiguous protein scaffold. *Proc Natl Acad Sci USA* 99: 15393–15397
- Poirier MG, Monhait T, Marko JF (2002) Reversible hypercondensation and decondensation of mitotic chromosomes studied using combined chemical-micromechanical techniques. *J Cell Biochem* 85: 422–434
- Rippe K (2012) The folding of the nucleosome chain. In *Genome organization and function in the cell nucleus*, Rippe K (ed.), pp 139–167. Weinheim: Wiley-VCH
- Robinson PJJ, Fairall L, Huynh VAT, Rhodes D (2006) EM measurements define the dimensions of the “30-nm” chromatin fiber: evidence for a compact, interdigitated structure. *Proc Natl Acad Sci USA* 103: 6506–6511
- de la Rosa-Trevín JM, Otón J, Marabini R, Zaldívar A, Vargas J, Carazo JM, Sorzano COS (2013) Xmipp 3.0: an improved software suite for image processing in electron microscopy. *J Struct Biol* 184: 321–328
- Sajan SA, Hawkins RD (2012) Methods for identifying higher-order chromatin structure. *Annu Rev Genomics Hum Genet* 13: 59–82
- Saurabh S, Glaser MA, Lansac Y, Maiti PK (2016) Atomistic simulation of stacked nucleosome core particles: tail bridging, the H4 tail, and effect of hydrophobic forces. *J Phys Chem B* 120: 3048–3060
- Schalch T, Duda S, Sargent DF, Richmond TJ (2005) X-ray structure of a tetranucleosome and its implications for the chromatin fibre. *Nature* 436: 138–141
- Scheffer MP, Eltsov M, Bednar J, Frangakis AS (2012) Nucleosomes stacked with aligned dyad axes are found in native compact chromatin *in vitro*. *J Struct Biol* 178: 207–214
- Scheres SHW, Melero R, Valle M, Carazo JM (2009) Averaging of electron subtomograms and random conical tilt reconstructions through likelihood optimization. *Structure* 17: 1563–1572
- Song F, Chen P, Sun D, Wang M, Dong L, Liang D, Xu RM, Zhu P, Li G (2014) Cryo-EM study of the chromatin fiber reveals a double helix twisted by tetranucleosomal units. *Science* 344: 376–380
- Stehr R, Schöpflin R, Etting R, Kepper N, Rippe K, Wederman G (2010) Exploring the conformational space of chromatin fibers and their stability by numerical dynamic phase diagrams. *Biophys J* 98: 1028–1037
- Strick R, Strissel PL, Gavrillov K, Levi-Setti R (2001) Cation-chromatin binding as shown by ion microscopy is essential for the structural integrity of chromosomes. *J Cell Biol* 155: 899–910
- Tang G, Peng L, Baldwin PR, Mann DS, Jiang W, Rees I, Ludtke SJ (2007) EMAN2: an extensible image processing suite for electron microscopy. *J Struct Biol* 157: 38–46
- Tatchell K, Van Holde KE (1978) Compact oligomers and nucleosome phasing. *Proc Natl Acad Sci USA* 75: 3583–3587
- Uberbacher EC, Bunick GJ (1985) X-ray structure of the nucleosome core particle. *J Biomol Struct Dyn* 2: 1033–1055
- Vilas JL, Gómez-Blanco J, Conesa P, Melero R, de la Rosa-Trevín JM, Otón J, Cuenca J, Marabini R, Carazo JM, Vargas J, Sorzano COS (2018) MonoRes: automatic and accurate estimation of local resolution for electron microscopy maps. *Structure* 26: 1–8
- White CL, Suto RK, Luger K (2001) Structure of the yeast nucleosome core particle reveals fundamental changes in internucleosome interactions. *EMBO J* 20: 5207–5218
- Widom J, Klug A (1985) Structure of the 300 Å chromatin filament: X-ray diffraction from oriented samples. *Cell* 43: 207–213
- Widom J (1986) Physicochemical studies of the folding of the 100 Å nucleosome filament into the 300 Å filament. Cation dependence. *J Mol Biol* 190: 411–424
- Wong H, Victor JM, Mozziconacci J (2007) An all-atom model of the chromatin fiber containing linker histones reveals a versatile structure tuned by the nucleosome repeat length. *PLoS One* 9: e877
- Wu C, McGeehan JE, Travers A (2016) A metastable structure for the compact 30-nm chromatin fibre. *FEBS Lett* 590: 935–942
- Zhou BR, Jiang J, Ghirlando R, Norouzi D, Yadav KNS, Feng H, Wang R, Zhang P, Zhurkin V, Bai Y (2018) Revisit of reconstituted 30-nm nucleosome arrays reveals an ensemble of dynamic structures. *J Mol Biol* 430: 3093–3110